TECHNIUM

Romanian Journal of Applied Sciences and Technology
ISSN: 2668-778X

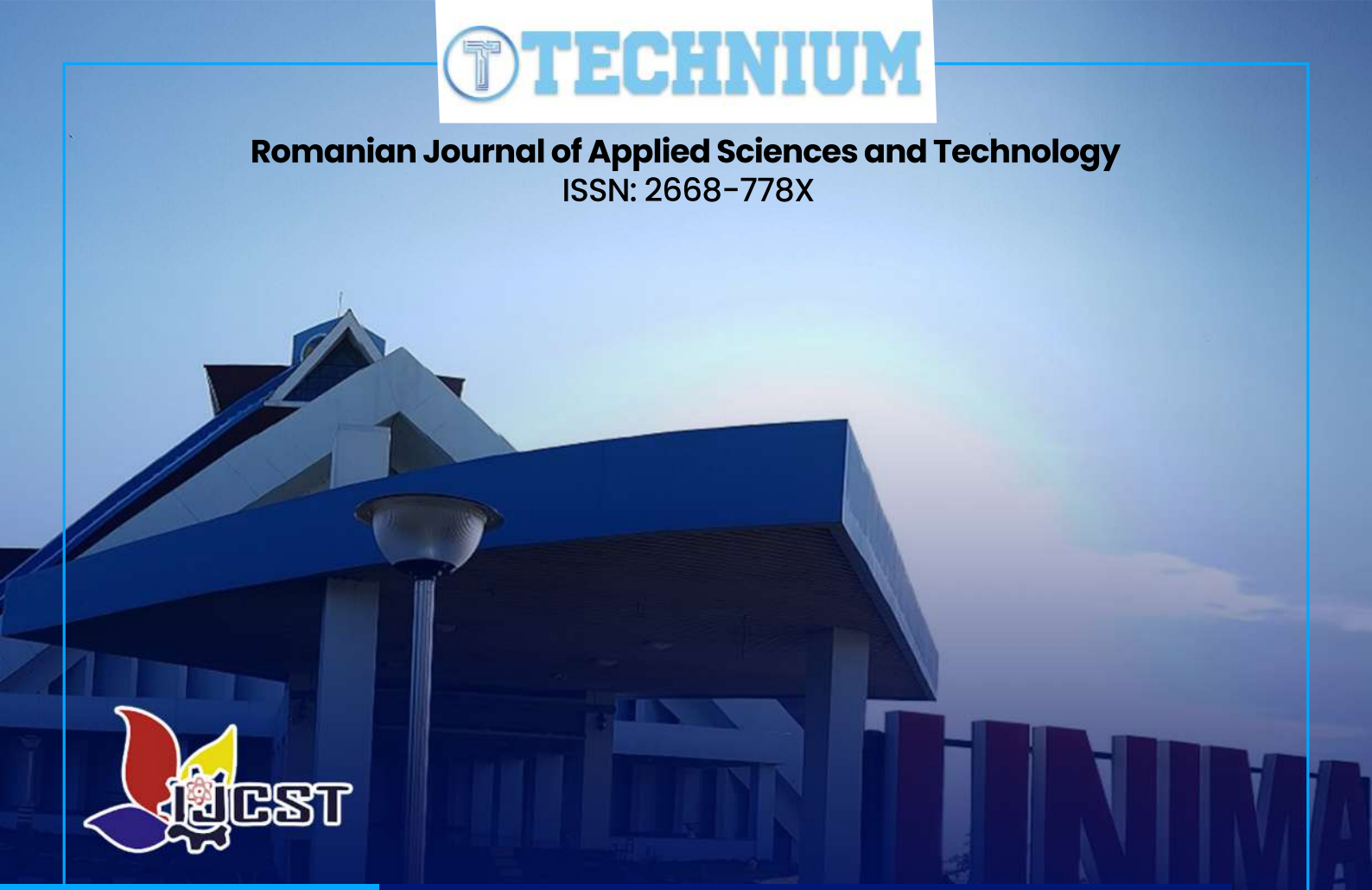

vol. 16 / 2023

The 7th International Conference on Science Technology

organized by
Faculty of Social Science and
Law Universitas Negeri Manado and
Consortium of International Conference
on Science and Technology

The Innovation Breakthrough in Digital and Disruptive Era

Technium: Romanian Journal of Applied Sciences and Technology
Vol. 16, 405-410, October, 2023
ISSN: 2668-778X
www.techniumscience.com

Crystallography Analysis on LSCF and LSM-based Perovskite Oxides

Silvana Dwi Nurherdiana[1,2*], *Nikmatin Sholichah*[3], *Susilowati*[1,2], *Sukirmiyadi*[2], *Erwan Adi Saputro*[1,2], *Mohd Jumain Jalil*[4] and *Hamzah Fansuri*[5]

[1] Master of Environmental Science, Faculty of Engineering and Sciences, Universitas Pembangunan Nasional Veteran Jawa Timur, Indonesia
[2] Study Program of Chemical Engineering, Faculty of Engineering and Sciences, Universitas Pembangunan Nasional Veteran Jawa Timur, Indonesia
[3] Study Program of Physics, Faculty of Mathematics and Sciences, Universitas Billfath, Indonesia
[4] Chemical Engineering Studies, College of Engineering, Universiti Teknologi Mara Johor Branch, Pasir Gudang Campus, Malaysia
[5] Department of Chemistry, Faculty of Science and Data Analytics, Institut Teknologi Sepuluh Nopember, Indonesia

Abstract. Perovskite oxide as a metal oxide offers an excellence on mixed ionic and electronic conductor (MIEC) properties which work simultaneously. The crystal structure of perovskite oxide plays the important role to achieve the superior performance. Generally, it formed a cubic which potentially distorted due to the ratio of metal ion constituents, the calcination temperature and the synthesis method used. Thus, this study presents chemical analysis of $La_{0.7}Sr_{0.3}Co_{0.2}Fe_{0.8}O_{3-\delta}$ (LSCF) and $La_{0.7}Sr_{0.3}MnO_{3-\delta}$ (LSM)-based perovskite oxides through crystallographic identification using Rietveld Refinement method (Rietica software) and material porosity analysis. The results show that the two types of perovskite oxide have different distorted crystal structures. Perovskite oxide LSCF produces hexagonal crystals and 63.98% rhombohedral dominance, while LSM remained significantly different from LSCF. LSM consist less hexagonal and 55.47% cubic structure. In addition, the pore characteristics indicate that macropores and pore volumes are more abundant in LSCF than LSM. This information can be used as a basis for the use of oxide materials as a separator of oxygen ions from the air, solid oxide fuel cells and catalyst for value-added chemical production from methane flue gas.

* Corresponding author: silvana.dwi.tk@upnjatim.ac.id

TECHNIUM

Technium: Romanian Journal of Applied Sciences and Technology
Vol. 16, 405-410, October, 2023
ISSN: 2668-778X
www.techniumscience.com

1 Introduction

Generally, a perovskite oxide has an ABO_3 type crystal structure, where A-site cation from rare earth, alkaline earth, alkali and other large ions such as La^{3+} which fit into the dodecahedral site. B-site cation filled by 3d, 4d, 5d, or transition metal ions (Mn, Co, Fe, Ni, Ti), which occupy the octahedral sites of the framework [1, 2]. A perovskite oxide received much attention over the past decade. Their activity and thermal stability have been extensively applied as catalyst for the partial oxidation of methane with controlled O_2 [3].

Perovskite presented mixed ionic-electronic conducting (MIEC) properties, namely the ability to diffuse oxygen ions (O^{2-}) and electrons simultaneously. The presence of a cation with a large ionic radius causes a change in the electronic properties and the formation of oxygen vacancies which in turn increase the mobility of oxygen ions [4].

In MIEC, oxygen passes through the material from high to low pressure. Oxygen gas on the high pressure side absorbed by the surface of the material and dissociated into oxygen ions which filled the oxygen vacancies in the MIEC crystal. The formation of oxygen ions occurs by absorbing electrons from the material. Furthermore, the oxygen ions that are formed migrate to the other side which has a low oxygen pressure. At the same time, the metal ion on the B-side of the perovskite is oxidized to a higher valence state by releasing electrons to balance the local charges. Electron conduction from the B cation lattice is obtained from the B-O-B bond through the Zerner double exchange mechanism as shown in the following reaction:

$$B^{n+} - O^{2-} - B^{(n+1)+} \rightarrow B^{(n+1)+} - O^{-} - B^{(n+1)+} \rightarrow B^{(n+1)+} - O^{2-} - B^{n+} \quad (1)$$

Oxygen ions undergo oxidation to become oxygen on the surface of the material under low oxygen pressure which then desorption from the surface and diffuses into the gas phase [5].

In ABO_3 perovskites, the catalytic activity can be enhanced by partial substitution on A-site and B-site. In addition, the binding energy of the B-O bond is the important factor controlling the catalytic properties. $LaSrCoO_{3-\delta}$ perovskite oxide as a type of catalyst has the oxygen mobility property, which means that the oxygen can leave the structure without deforming structure. As previous research revealed that the perovskite $La_{0.7}Sr_{0.3}CoO_{3-\delta}$ have structure phase crystal and have good thermal stability until 900 °C [6, 7]. On the other hand, there have been few reports which have dealt with the effect of B-site substitution [8]. It was found that in the perovskite oxide structure with partial substitution of Co^{3+} by Fe^{2+} positively affect the catalytic activity significantly [9].

Therefore, this research aims to analysis the chemical structure different A and B-site of perovskite oxie of $La_{0.7}Sr_{0.3}Co_{0.2}Fe_{0.8}O_{3-\delta}$ (LSCF) and $La_{0.7}Sr_{0.3}MnO_{3-\delta}$ (LSM) through crystallographic identification using Rietveld Refinement method (Rietica software) and material porosity analysis using Brunauer-Emmett-Teller (BET) method. The effect of B-site partial substitution of perovskite-type was revealed from X-ray diffraction (XRD) and N_2 adsorption.

2 Experimental

2.1 Materials

Metal oxide and carbonate-based chemicals in powder form used for the preparation of perovskite $La_{0.7}Sr_{0.3}Co_{0.2}Fe_{0.8}O_{3-\delta}$ (LSCF 7328) and $La_{0.7}Sr_{0.3}MnO_{3-\delta}$ (LSM 73), were supplied from Sigma-Aldrich. Lanthanum (III) oxide (La_2O_3) has a purity of ≥99.9%, cobalt (III) oxide (Co_3O_4) p.a ≥99%, strontium carbonate ($SrCO_3$) ≥99.9%, iron (III) oxide (Fe_2O_3) p.a ≥99% and manganese (II) carbonate ($MnCO_3$) p.a 99.9%. The two perovskite oxides were prepared using a solid-state based method (solid-solid reaction) as described in the literature [1, 10]

2.2 Synthesis of LSCF and LSM-based Perovskite Oxides

First, the metal oxides and carbonates were dried in an oven at 105 °C for 1 hour to remove moisture, then followed by cooled under vacuum in a desiccator for 24 hours. Each powder was weighed according to the composition and then poured into a different mortar to be crushed for 2 hours using a ball mill with 600 rpm at room temperature. The obtained powder is then calcined gradually from 400 to 1000 °C for 2 h of each calcination temperature to form a perovskite structure.

The grinding stage is carried out at the end of each stage for 15 minutes to increase the heating area thereby reducing the risk of secondary phase formation other than perovskite. In the final stage, the perovskite is sieved at 400 mesh to make the grain size uniform. The colour change of the powder from red to black under the conditions before and after calcination is shown in Figure 1.

(a) (b)

Fig. 1. Images of Colour Change of Powder before (a) and after Calcination (b).

2.3 Crystallography Analysis and Characterizations

Crystallography analysis aims to determine the phase structure and crystal characteristics of the catalyst, which are measured at room temperature with an X-ray source. XRD analysis at room temperature used the PANalytical Expert system instrument (diffractometer type: Xpert MPD). The detailed

Technium: Romanian Journal of Applied Sciences and Technology
Vol. 16, 405-410, October, 2023
ISSN: 2668-778X
www.techniumscience.com

measurement conditions during measurement are shown in Table 1.

Table 1. Parameters of Diffraction Analysis Conditions at Room Temperature.

2θ (°)	: 5,0084 – 99,9874
Step size 2θ (°)	: 0,0170
Specimen length (mm)	: 10
Observation time (s)	: 10,1500
Measurement temperature (°C)	: -273,15
Anode Materials	: Cu
K-α1 (Å)	1,54060
K-α2 (Å)	1,54443
K-β (Å)	1,39225
Ratio of K-α1/ K-α2	0,5000
Generator settings and tube current	: 30 mA, 40 kV

The diffractogram obtained was then processed using the Rietveld refinement method using Rietica software to obtain the percentage value of the crystalline phase and lattice parameters such as a, b, c, α, β, γ and lattice volume [11]. The Rietveld refinement structure model is taken from the Powder Diffraction File (PDF) data which is shown in detail in Table 2.

Table 2. Perovskite oxide structure reference LSCF and LSM.

PDF Number	Molecular Formula	Crystal Shape	Lattice Size (Å)			Lattice Angle (°)		
			a	b	c	α	β	γ
00-082-1963	$La_{0.4}Sr_{0.6}FeO_3$	R-3c:H (167) (Hex)	5.4937		13.4106	90		120
00-086-1665	LaCoO3	R-3c:R (167) (Rh)	5.5150			90		
00-047-0444	$La_{0.9}Sr_{0.1}MnO_3$	R-3c:H (167) (Hex)	5.5336		13.3560	90		120
00-075-0440	$LaMnO_3$	Pm-3m (221) (Cub)	3.8800			90		

Diffractogram data processing through the Rietveld refinement method is carried out using Rietica software. In addition, the model and lattice parameters must be set as close as possible to the actual value that has been agreed upon as the value of Goodness of fit (Gof) or quality factor with a value of $\chi 2 < 2$, $Rp < 15$ and $Rwp < 15$ [12]. In this study, the zero offset starts from an angle of 2θ: -0.049°, the values of V: -0.01200 and W : 0.02100 are obtained from the characteristics of the instruments. After the crystal structure was obtained, the surface area and particle size were determined by the BET method using N_2 gas as an adsorbate at liquid N_2 temperature (-195.69 °C).

3 Result and Discussions

The LSCF and LSM diffractograms and the reference phases were shown in Figure 2 and 3, respectively. Based on phase similarity analysis using Match! software, LSCF perovskite oxide showed good phase similarity with Powder diffraction file (PDF) model number 00-086-1665 for hexagonal $La_{0.4}Sr_{0.6}FeO_3$ and 00-082-1963 for rhombohedral $LaCoO_3$. This confirms that the synthesized LSCF consists of two structures.

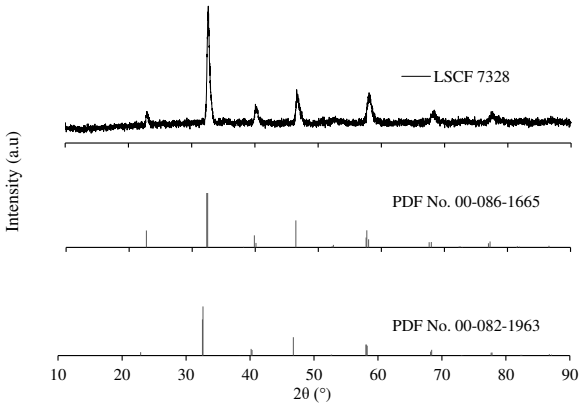

Fig. 2. Diffractogram of $La_{0.7}Sr_{0.3}Co_{0.2}Fe_{0.8}O_{3-\delta}$ and reference phase information from PDF numbers 00-086-1665 and 00-082-1963.

The LSM perovskite oxide shows good similarity with reference phase PDF number 00-047-0444 for hexagonal $La_{0.9}Sr_{0.1}MnO_3$ and 00-075-0440 for cubic $LaMnO_3$. The percentage of the two phases present in the powder can be further known through processing using the Rietveld refinement method.

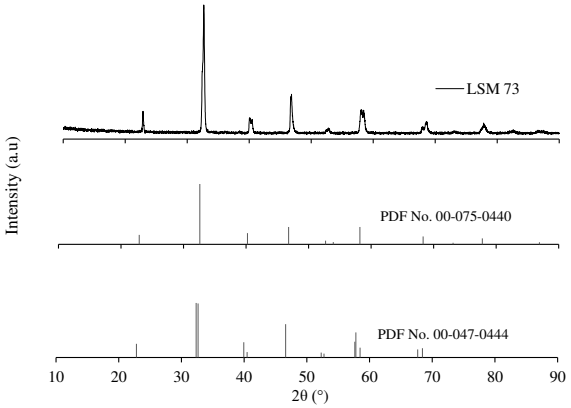

Technium: Romanian Journal of Applied Sciences and Technology
Vol. 16, 405-410, October, 2023
ISSN: 2668-778X
www.techniumscience.com

Fig. 3. Diffractogram of $La_{0.7}Sr_{0.3}MnO_{3-\delta}$ and reference phase information from PDF numbers 00-075-0440 and 00-047-0444.

The results of the Rietveld refinement processing using the Rietica software from room temperature XRD analysis are shown in Figure 4. The processing results show that the diffractogram closely matches the reference phase used as a model. This is qualitatively shown by the red (model) as the experimental data and black (sample diffractogram) fitting lines which are aligned from Rietveld refinement, the Bragg peaks (blue) and the difference values (green) which tend to make it look like a straight line.

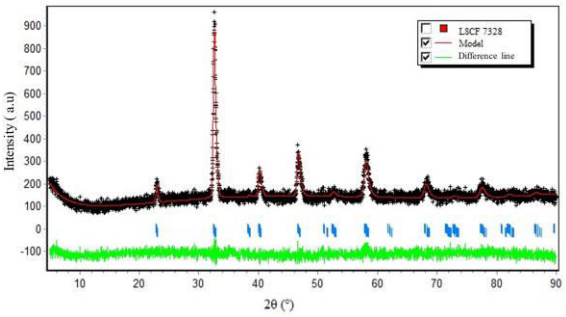

(a)

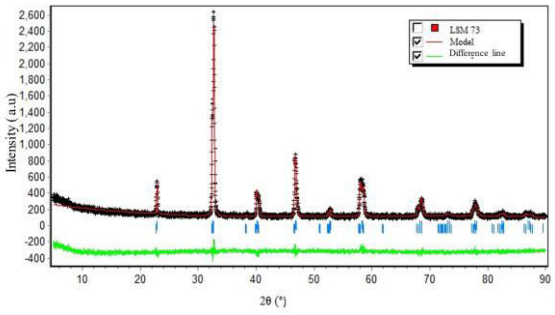

(b)

Fig. 4. Rietveld refinement results of perovskite oxide LSCF (a) and LSM (b) using Rietica software.

Quantitatively, the fit between the model and the sample diffractogram is indicated by the quality factor values including the R-structural factor (Rp) and weighted pattern (Rwp) less than 20% and goodness of fit (x2) less than 10% as shown in Table 3.

Table 3. The quality factor of LSCF and LSM diffractogram data processing uses the Rietveld refinement method (Rietica software).

Quality Factor	LSCF	LSM
R-structure factor (Rp) (%)	7.588	8.619
Weighted residual (Rwp) (%)	9.605	10.936
Goodness of fit (x^2) (%)	1.379	1.951

The lattice size values from the results of the Rietveld refinement diffractogram at room temperature are tabulated in Table 4. The results show that the synthesized LSCF has a larger hexagonal phase lattice size compared to the reference phase (a=b 5.4936 Å and c 13.4106 Å) while the rhombohedral phase has a slightly smaller value than the reference phase (a=b=c 5.5150 Å). The LSM lattice size values obtained show that the lattice size values of the two phases are calculated to be slightly smaller than the reference phase values. The lattice size values for the hexagonal reference phase are a=b 5.5336 Å and c 13.3560 Å and the cubic reference phase is a=b=c 3.8800 Å.

Table 4. Lattice parameters from the refinement of LSCF and LSM diffractograms.

	LSCF		LSM	
Space group	R-3c (167) Hexagonal	R-3c (167) Rombohedral	R-3c (167) Heksagonal	Pm-3m (221) Cubic
Percentage of phase weight (%)	36.02	63.98	44.53	55.47
Derived bragg R-factor (%)	2.51	2.09	3.20	2.59
Lattice size (Å)				
a:	5.5202	5.4846	5.51458	3.8704
b:	5.5202	5.4846	5.51458	3.8704
c:	13.4786	5.4846	13.3553	3.8704
Lattice volume ($Å^3$)	355.7024	116.2025	351.7307	57.9784

This shows that the differences in the composition of the metals affected the perovskite structures that tend to be distorted to hold on to a stable structure. From the processing data, it was found that the weight percentage between the two phases, namely the LSCF hexagonal LSCF: rhombohedral was 36.02 %: 63.98 % which indicated that the rhombohedral phase was more dominant while the weight of the LSM phase was more dominated by the cubic phase of 55.47% compared to the hexagonal phase of 44.53%.

Images of crystal structures and atomic coordinates were studied further using x-ray diffraction analysis data at room temperature by processing using Rietica software equipped with Powdercell (PCW) processing results. The crystal structure equipped with the bond lengths between atoms in the LSCF perovskite oxide is shown in Figure 5 while the LSM is shown in Figure 6. Both perovskite oxides have hexagonal phase symmetry but LSM has a shorter bond length. This proves that the radius of the Mn^{3+} ion is lower than that of Fe^{3+} and Co^{2+} which affects the bond length between atoms in the arrangement of crystal structures.

Technium: Romanian Journal of Applied Sciences and Technology
Vol. 16, 405-410, October, 2023
ISSN: 2668-778X
www.techniumscience.com

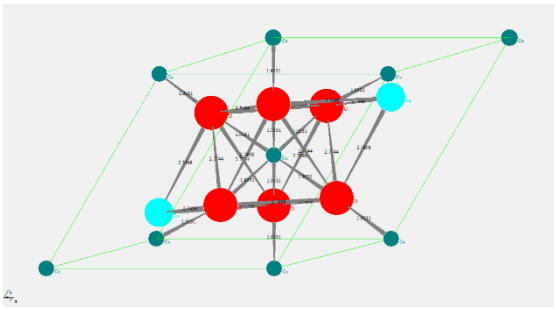

(a) LSCF Hexagonal

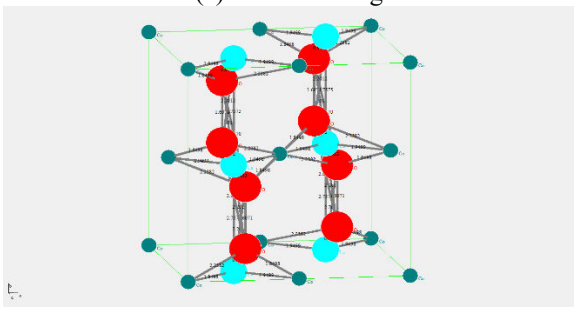

(b) LSCF Rhombohedron

Fig. 5. Crystal structure and bond length of the LSCF perovskite oxide on the 001 plane.

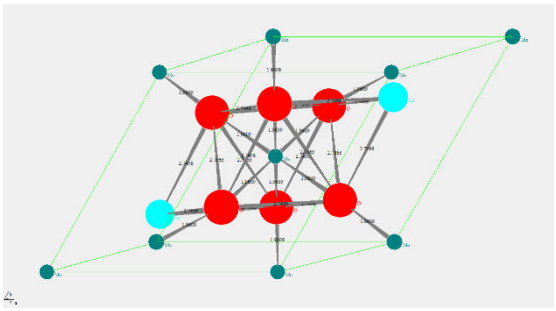

(a) LSM Hexagonal

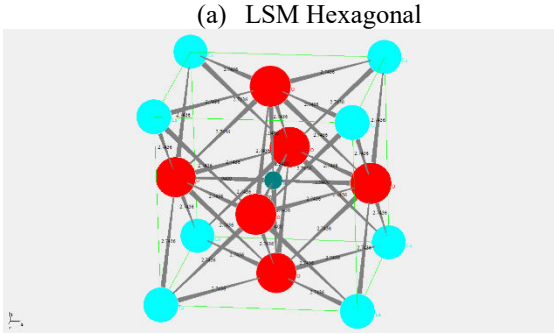

(b) LSM Cubic

Fig. 6. Crystal structure and bond length of the LSM perovskite oxide in the 001 plane

The next analysis that has been carried out is adsorption of nitrogen isotherms using the BET method which provides further information regarding the pore characteristics of the catalyst. Table 5 shows the results of the analysis of the specific surface area and pore size distribution of LSCF 7328 and LSM 73. The BET surface area of LSCF is 5.0763 $m^2.g^{-1}$, which is three times larger than that of LSM 73. This value can be attributed to the smaller pore size of LSCF compared to the pore size of LSM. The surface area value obtained has a lower agglomeration potential as described by Ahmad et al [13]. Agglomeration initiates clumping when the powder used as a suspension solution so that it can cause inhomogeneity which further damages the configuration or other characteristics of the membrane.

Table 5. Specific surface area and pore size distribution of perovskite oxide LSCF and LSM.

Perovskite oxide powder	Specific surface area ($m^2.g^{-1}$)	Pore volume ($cm^3.g^{-1}$)	Average pore diameter (Å)
LSCF	5.0763	0.004789	37.7384
LSM	1.6017	0.002796	69.8264

Figure 7 represents nitrogen adsorption isotherm curve measured using the BET method. The results can be used to qualitatively determine the adsorption mechanism. Based on the International Union of Pure and Applied Chemistry (IUPAC) classification, the adsorption curves of LSCF and LSM are type II adsorption, which are normal forms of isotherms obtained from non-porous or macroporous adsorbent materials. The first almost linear starting point and the middle part of the isotherm indicate the completion of the monolayer stage and the multilayer adsorption begins.

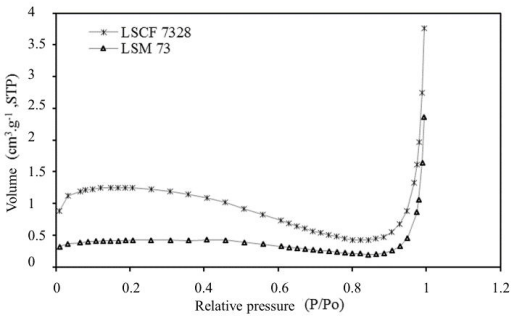

Fig. 7. Isotherm nitrogen adsorption curves using the BET method on LSCF and LSM.

Furthermore, the pore size distribution was determined by nitrogen adsorption-desorption using the BJH method. The BJH method is used to analyze materials that have large pore sizes as shown in Figure 8. LSCF perovskite oxide has a more macropore size distribution compared to LSM. This is evidenced by the statement of Ahmad et al which stated that a pore diameter greater than 500 Å represents a macro pore size character [13, 14].

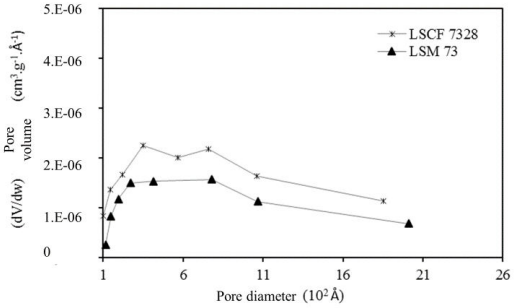

Fig. 8. Pore size distribution curve using the BJH method on LSCF and LSM.

4 Conclusions

The LSCF and LSM-based perovskite oxides were successfully synthesized by solid-state method. This method represents different chemical characteristics namely crystallography and specific surface area as affected different B-site of Co^{3+}, Fe^{3+} and Mn^{2+}. The value of the Goldschmidt tolerance factor influenced by the size value of the metal ion, for which LSCF and LSM use several different metal ions.

References

1. Nurherdiana S.D., Sholichah N., Iqbal M.R., Sahasrikirana M.S., Utomo W.P., Akhlus S., Nurlina N., Fansuri H.: Preparation of $La_{0.7}Sr_{0.3}Co_{0.2}Fe_{0.8}O_{3-\delta}$ (LSCF 7328) by Combination of Mechanochemical and Solid State Reaction Key Engineering Materials. pp. 399–403 (2017)
2. Ghouse M., Al-Yousef Y., Al-Musa A., Al-Otaibi M.F.: Preparation of $La_{0.6}Sr_{0.4}Co_{0.2}Fe_{0.8}O_3$ nanoceramic cathode powders for solid oxide fuel cell (SOFC) application Int. J. Hydrogen Energy, 35, pp. 9411–9419 (2010)
3. Fansuri H., Masyitoh A.D., Nurherdiana S.D., Utomo W.P., Gunawan T., Widiastuti N., Othman M.H.D., Ismail A.F., Subaer: A dependence study: Molecular weight of polyethylene glycol (PEG) ON $La_{0.7}Sr_{0.3}Co_{0.2}Fe_{0.8}O_{3-\delta}$ (LSCF 7328) hollow fiber membrane for oxygen permeation J. King Saud Univ. - Eng. Sci., 35, pp. 200–206 (2023)
4. Möbius A., Henriques D., Markus T.: Sintering behaviour of $La_{1-x}Sr_xCo_{0.2}Fe_{0.8}O_{3-\delta}$ ($0.3 \leq x \leq 0.8$) mixed conducting materials J. Eur. Ceram. Soc., 29, pp. 2831–2839 (2009)
5. Shao Z., Xiong G., Cong Y., Yang W.: Synthesis and oxygen permeation study of novel perovskite-type $BaBixCo_{0.2}Fe_{0.8-x}O_{3-\delta}$ ceramic membranes 164, pp. 167–176 (2000)
6. Dunyushkina L.A.: Solid Oxide Fuel Cells with a Thin Film Electrolyte: A Review on Manufacturing Technologies and Electrochemical Characteristicses Electrochem. Mater. Technol., 1, pp. 20221006 (2022)
7. Liu P., Liu Z., Wu P., Ou X., Zhang Y., Cai W., Yu F., Ni M., Cheng S., Liu M., Liu J.: Enhanced capacitive performance of nickel oxide on porous $La_{0\cdot7}Sr_{0\cdot3}CoO_3$ ceramic substrate for electrochemical capacitors Int. J. Hydrogen Energy, 43, pp. 19589–19599 (2018)
8. Fansuri H., Syafi'i M.I., Romdoni S., Masyitoh A.D., Utomo W.P., Prasetyoko D., Widiastuti N., Murwani I.K., Subaer: Preparation of dense $Ba_xSr_{1-x}Co_{0.8}Fe_{0.2}O_3$ membranes: Effect of Ba2+ substituents and sintering method to the density, hardness and thermal expansion coefficient of the membranes Adv. Mater. Lett., 8, pp. 799–806 (2017)
9. Iqbal R.M., Nurherdiana S.D., Hartanto D., Othman M.H.D., Fansuri H.: Morphological control of $La_{0.7}Sr_{0.3}Co_{0.2}Fe_{0.8}O_{3-\delta}$ and $La_{0.7}Sr_{0.3}MnO_{3-\delta}$ catalytic membrane using PEG-H_2O additive IOP Conference Series: Materials Science and Engineering. vol. 348. Institute of Physics Publishing (2018)
10. Utomo W.P., Ilham A.M., Khoiroh N., Nurherdiana S.D., Pasicakti G.P., Swtyawati M.Z., Fansuri H.: Comparison Of $La_{0.6}Sr_{0.4}Co_{0.2}Fe_{0.8}O_3$ Perovskite Synthesis Methods And Their Effect On The Particle Size Rasayan J. Chem., 12, pp. 697–706 (2019)
11. Adroja D.T., Bhattacharyya A., Sato Y.J., Lees M.R., Biswas P.K., Panda K., Anand V.K., Stenning G.B.G., Hillier A.D., Aoki D.: Pairing symmetry of an intermediate valence superconductor $CeIr_3$ investigated using μsR measurements Phys. Rev. B, 103, (2021)
12. Fitriana F., Baity P.S.N., Zainuri M., Kidkhunthod P., Suasmoro S.: Crystal structure and Cu/Fe K-edge analysis of $Ba_{0.5}Sr_{0.5}Fe_{1-x}Cu_xO_{3-\delta}$ ($x = 0–0.2$) and the influence on conductivity J. Phys. Chem. Solids, 154, pp. 110065 (2021)
13. Ahmad S.H., Jamil S.M., Othman M.H.D., Rahman M.A., Jaafar J., Ismail A.F.: Co-extruded dual-layer hollow fiber with different electrolyte structure for a high temperature micro-tubular solid oxide fuel cell Int. J. Hydrogen Energy, 42, pp. 9116–9124 (2017)
14. Nurherdiana S.D., Gunawan T., Widiastuti N., Fansuri H.: Grand Challenges of Perovskite and Metal Oxide-based Membrane: A Form of Dual-layer Hollow Fibre J. Appl. Membr. Sci. Technol., 25, pp. 17–28 (2021)